ARTICLES

Ionization and Emission Spectra of the Photofragments of Allene Excited at 193 nm

Jia-lin Chang,[†] Gi-chen Tseng,[‡] Chi-Kung Ni,[†] Jiahn-Dar Huang,[‡] and Yit-Tsong Chen*[,†,‡]

Institute of Atomic and Molecular Sciences, Academia Sinica, P.O. Box 23-166, Taipei 106, Taiwan, ROC, and Department of Chemistry, National Taiwan University, Taipei 106, Taiwan, ROC

Received: January 5, 1999; In Final Form: April 12, 1999

The ionic and luminous photofragments of allene excited with a single focused laser beam at 193 nm are detected using time-of-flight mass spectrometry and dispersed emission spectroscopy, respectively. The major ionic products detected are C_3^+, C_2^+, and C^+. The yields of $C_3H_n^+$ ($n = 1-3$) are minor compared to the carbon ions. For the emission spectra, the C_2 Swan system ($d^3\Pi_g \rightarrow a^3\Pi_u$), the C_2 Mulliken system ($D^1\Sigma_u^+ \rightarrow X^1\Sigma_g^+$), CH($A^2\Delta \rightarrow X^2\Pi$), and an atomic line corresponding to the C($2p3s\ ^1P^o$) → C($2p^2\ ^1S$) transition are the major features observed. The vibrational population in the $C_2(d^3\Pi_g)$ state is found inverted to a thermal equilibrium distribution. The laser-power dependence of each photofragment is measured, from which multiphoton dissociation and ionization mechanisms of allene are proposed. A kinetic model is developed to further illuminate the photodissociation mechanisms. Although C_n^+ ($n = 1-3$) ions are the major species observed in the present photodissociation experiment, $C_3H_n^+$ ($n = 1-4$) are most abundant in the electron impact of allene. The hydrogen elimination and carbon−carbon bond rupture in the photodissociation of allene at 193 nm, with C_n and C_3H_n ($n = 1-3$) photofragments, are concluded to precede the competing multiphoton ionization process, in producing $C_3H_4^+$, within the laser flux ($<2.7 \times 10^{26}$ photons cm^{-2} s^{-1}) used in this experiment.

1. Introduction

Allene ($H_2C{=}C{=}CH_2$) is an important hydrocarbon in combustion chemistry and astrophysics because of its role as a precursor of many key species, such as C_3H_3, C_3H_2, C_3H, and C_3. For instance, C_3H_3 has been discovered to play a role in soot formation in combustion processes.[1−3] C_3H_2 and C_3H have been observed in many interstellar mediums.[4−10] C_3 is well-known for its importance in cometary science.[11] The isomerization of C_3H_n ($n = 1-4$) among different isomers has also attracted many theoretical and experimental studies.[12−21] A substantial body of infrared and microwave spectroscopy of these species has been investigated in the past decades.[4−10,22−27] However, electronic spectroscopy[28−31] results and studies of the photodissociation dynamics for allene and its photofragments are scanty.

Jackson et al.[32] and Sun et al.[33] measured the translational energy distribution of the photofragments of allene at 193 nm in a molecular beam. According to their results, C_3H_3 and C_3H_2 are the major products in the primary dissociation. Under a similar experimental condition, Song et al. reported the same internal state distribution of C_3 resulting from the photolysis of the geometric isomers of allene and propyne using laser-induced fluorescence spectroscopy.[34] They proposed that C_3 is produced via the secondary photodissociation from the fragment of C_3H_2. Mebel and co-workers performed ab initio calculations for the electronic states of C_3H_n ($n = 1-4$) to investigate a variety of dissociation channels.[35,36] Our most recent experimental study[37] has demonstrated that the primary photodissociations of allene and propyne are markedly different and that no isomerization occurs in the primary process.

This study detected the ionic and luminous photofragments of allene excited with a single focused ArF laser beam at 193 nm. According to the calculations,[35] three singlet excited electronic states of allene, $^1A_2$, $^1B_1$, and ^1E could absorb 193 nm photons, and the initial excitation is to a state allowed by vibronic interaction. An ArF laser served as a photodissociation and ionization light source in this study. Laser-power dependence measurements reveal the mechanisms accounting for the competition between dissociation and ionization in the excited states of allene and its photofragments. The major products observed are neutral carbons (C, C_2), carbon ions (C_3^+, C_2^+, C^+), and the hydrocarbon of CH. The yields of the hydrocarbon ions of $C_3H_n^+$ ($n = 1-4$) are relatively low compared with the yields of abundant carbon ions. All the observed products are generated by multiphoton processes. A kinetic model was developed to interpret the laser-power dependence of each photofragment and to illuminate the photodissociation/ionization mechanisms of allene.

The rest of this paper is organized as follows. Section 2 describes the experimental details. Section 3 presents the observed ionization and emission spectra and the laser-power dependence measurement for each photofragment. Next, section 4 provides a kinetic model for the photodissociation/ionization mechanisms of allene. Finally, conclusions are addressed in section 5.

* To whom correspondence should be sent. Address: Institute of Atomic and Molecular Sciences, Academia Sinica, P.O. Box 23-166, Taipei, Taiwan. E-mail: ytchen@pub.iams.sinica.edu.tw. Fax: +886 2-2362-0200.

[†] Institute of Atomic and Molecular Sciences.

[‡] Department of Chemistry, National Taiwan University.

10.1021/jp990045q CCC: $18.00
Published on Web 07/20/1999

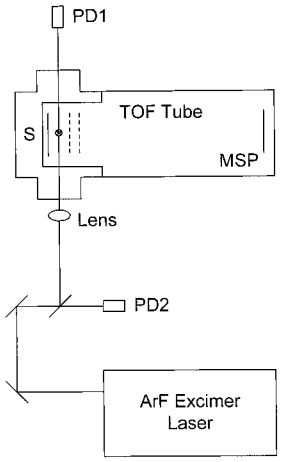

Figure 1. Schematic diagram of the experimental setup for time-of-flight mass spectrometry: MSP, microsphere plate; PD, photodiode; S, source chamber.

2. Experiment

2.1. Time-of-Flight Spectra. The experiment for the ionization spectroscopy of allene was performed using a time-of-flight (TOF) mass spectrometer. The TOF spectrometer consists of two vacuum chambers; one acts as a source chamber and the other provides room for photodissociation/ionization/TOF (Figure 1). The source chamber was evacuated to 1.3×10^{-6} Torr employing a turbomolecular pump (Seiko Seiki, STP-H1000C) backed with a mechanical pump (Edwards, E2M40). The molecular beam in this chamber was controlled by a pulsed valve (General Valve, 0.5 mm orifice) and was collimated downstream (3 cm) by a conical skimmer ($\phi \approx 1.3$ mm). The skimmed molecular beam, after a flight of 5 cm in the TOF chamber, interacts with a focused photodissociation/ionization laser beam. With differential pumping, the TOF chamber was evacuated to 2.7×10^{-7} Torr using another turbomolecular pump (Seiko Seiki, STP-400). A set of Wiley-McClaren plates[38] was used to accelerate ions, in the direction perpendicular to both molecular and laser beams, through the field-free TOF tube (50 cm). A microsphere plate (MSP, El-Mul) was used for the ion detection. The output signals from the MSP were recorded through the use of a digital oscilloscope (LeCroy, 9344); the recordings were then transferred to a personal computer for data acquisition.

The allene sample (Fluka, 90%) was vaporized and transferred into a cylinder in a vacuum system to remove the nonvolatile impurities. The sample was premixed with He (99.999%) to form a 10% mixture. The stagnation pressure was maintained at 2 atm by a pressure regulator. The purity of the mixed gas was ensured by an electron-impact ionization/quadrupole mass spectrometric examination. The pulse duration of the 10 Hz molecular beam was ~180 μs. The pressure in the source and the TOF chambers increased during operation to 1.5×10^{-5} and 4.5×10^{-6} Torr, respectively. The photodissociation/ionization laser beam (193 nm, 15 ns) is the output of an ArF excimer laser (Lumonics, EX-742). The laser was shaped by a circular iris ($\phi \approx 1.5$ cm) and focused into the chamber by a spherical lens ($f = 25$ cm). The focal area of the ArF laser was measured to be 0.6×0.2 mm^2 with 0−5 mJ/pulse. Under these experimental conditions, laser energy of 1 mJ corresponds to a flux of $\sim 5.4 \times 10^{25}$ photons cm^{-2} s^{-1} in the focal region. The time sequence between laser and molecular beams was controlled by a digital delay/pulse generator (Stanford Research, DG535).

2.2. Emission Spectra. The experiment for acquiring the dispersed emission spectra in the photodissociation of allene was performed in an evacuated stainless steel cell (~10^3 cm^3). The pressure of the flowing allene/He mixture, measured by a capacitance manometer (MKS, Baratron), was maintained at ~250 mTorr. The ArF laser was focused into the cell by a lens ($f = 20$ cm). The emitted light in the photodissociation of allene was directed at a right angle into a monochromator (Acton, SpectraPro-500) and was detected by a charge-coupled device (CCD) with 330 × 1100 pixels (Princeton Instruments, TE/CCD-1100PF/UV). The spectral dispersion was ~40 nm in a window frame of the CCD; thus, the resolution is $\sim 3.6 \times 10^{-2}$ nm/pixel. The spectral resolution in this experiment, however, was determined by the slit width of the monochromator and was measured to be 0.4−0.6 nm. A software (Princeton Instruments, CSMA) was used for controlling the gratings and acquiring dispersed emission spectra. Each spectrum was averaged for 200 laser shots.

2.3. Laser-Power Dependence of Photofragments. To derive the power dependence of the ionic photofragments, laser energy was measured using a photodiode and was calibrated applying an energy meter (Ophir, PE-50) at the entrance of the vacuum chamber following each experiment. Both the signal outputs from photodiode and MSP were integrated through the use of boxcar averagers (Stanford Research, SR250). The averaged signals were digitized by an A/D converter, and the digitized conversions were recorded using a personal computer in real time. Each data point was averaged for 10 measurements.

Specifically in the emission experiments, the power dependence of the luminous C_2 Swan system was measured by a photomultiplier tube (Hamamatsu, R943-02) screened with a glass filter (ESCO, GG-475) to collect emitting light of $\lambda \geq 475$ nm. For the C_2 Mulliken system, the CH($A^2\Delta \rightarrow X^2\Pi$) transition and the atomic transition of C($2p3s\ ^1P^o$) → C($2p^2\ ^1S$), laser-power dependencies were analyzed from the peak areas in dispersed emission spectra. The laser energy was calibrated in a similar way as the ionic photofragments were calibrated, as previously described.

The excited photofragments, responsible for the observed emission spectra in the present experiment, were produced via a collisionless process. The support for this interpretation was obtained by examining the temporal behavior of the emission. Within the time resolution of the photomultiplier tube (rise time of ~3 ns), the signal directly followed the laser pulse.

3. Results

3.1. TOF Spectra. A typical TOF spectrum for the excitation of allene at 193 nm is demonstrated in Figure 2. The major ionic products are C_3^+, C_2^+, and C^+. The yields of $C_3H_n^+$ ($n = 1-3$) are minor compared with the carbon ion yield. A small amount of C_2H^+ is also observed. The signals of the parent molecular ion ($C_3H_4^+$) and the hydrogen ion (H^+) are very small and were observed only occasionally within the laser flux (<2.7×10^{26} photons cm^{-2} s^{-1}) used in this experiment.

3.2. Emission Spectra. The dispersed emission spectra taken in the photodissociation of allene excited with a focused 193 nm laser beam are displayed in Figure 3. These spectra can be divided into four categories:[39−42] (a) the C_2 Mulliken system ($D^1\Sigma_u^+ \rightarrow X^1\Sigma_g^+$) at 231 nm; (b) an atomic line corresponding to C($2p3s\ ^1P^o$) → C($2p^2\ ^1S$) at 247.9 nm (Figure 3a), which is much narrower than any other band observed in this experiment; (c) the CH($A^2\Delta \rightarrow X^2\Pi$) transition degraded to the violet and headed at 431 nm; (d) the most intense C_2 Swan system ($d^3\Pi_g \rightarrow a^3\Pi_u$) from 430 to 630 nm (Figure 3b). The famous cometary bands of C_3 around 405 nm were not observed.[11] The emission

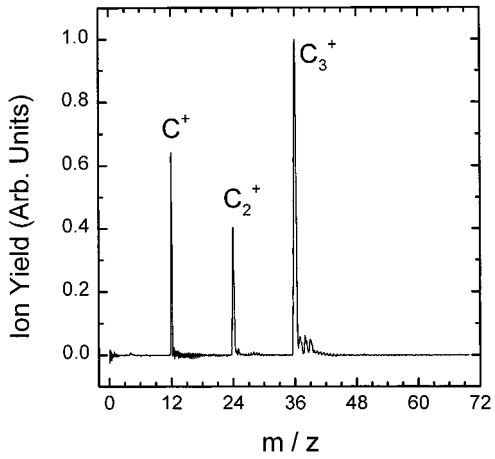

Figure 2. Typical time-of-flight mass spectrum of allene excited at 193 nm.

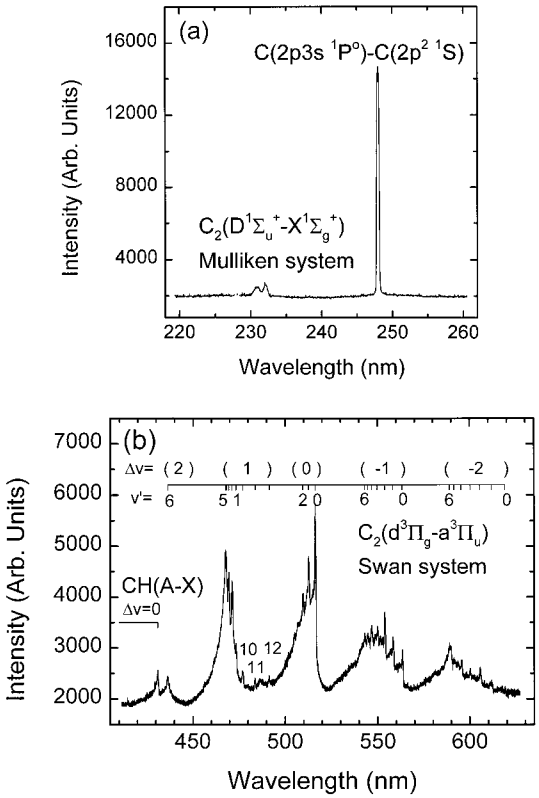

Figure 3. Dispersed emission spectra of allene excited at 193 nm.

band at 231 nm has been identified as belonging to the C_2 Mulliken system rather than the C_2H_2 $A^1A_u \rightarrow X^1\Sigma_g^+$ transition according to a simulated spectral line shape obtained by using well-determined spectroscopic constants. The assignment for the CH($A^2\Delta \rightarrow X^2\Pi$) transition is also based on a simulated line shape of the corresponding transition. Moreover, the slope of 1.8 in the laser-power dependence for this peak is different from that of 3.0 for the nearby C_2 Swan system, as will be discussed in section 4.2.

Each peak of the C_2 Swan system can be definitely assigned as displayed in Figure 3b.[39] The spectrum primarily consists of five vibrational sequences (i.e., $\Delta v = -2, -1, 0, 1, 2$) corresponding to the transitions between the $d^3\Pi_g$ and $a^3\Pi_u$ states of C_2. The highest vibrational level of the $C_2(d^3\Pi_g)$ state observed in this experiment is $v' = 12$. The relative vibrational population distribution up to $v' = 6$ in the $C_2(d^3\Pi_g)$ state is determined as depicted in Figure 4. The population is calculated

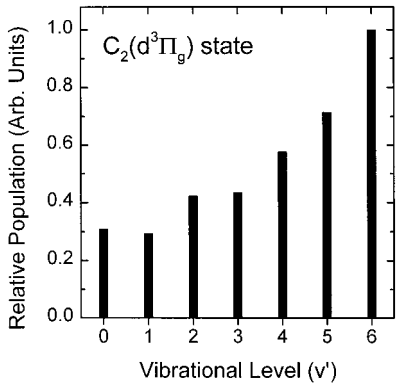

Figure 4. Vibrational population distribution of the $C_2(d^3\Pi_g)$ photofragment.

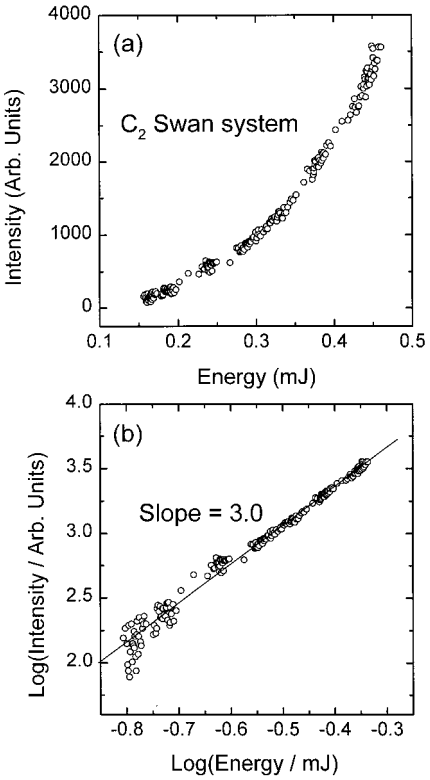

Figure 5. Laser-power dependence of the $C_2(d^3\Pi_g)$ photofragment. The solid line in (b) is a linear fit of the experimental data.

from the same sequence ($\Delta v = -1$) where the peaks for analysis are well resolved. The population is obtained from the band-head intensities divided by the Franck−Condon factors[43] and the frequency factor of ν^3. The calculated population also agrees with the results from other sequences ($\Delta v = 0$ and -2) where fewer peaks were resolved. The vibrational population in $C_2(d^3\Pi_g)$, as depicted in Figure 4, is found to be inverted to a thermal equilibrium distribution. The vibrational distribution from $v' = 7$ to $v' = 12$ is not attempted in the present study because these bands are headless and seriously overlapped each other under the spectral resolution in this study.

3.3. Laser-Power Dependence of Photofragments. We have measured the laser-power dependence of each ionic and luminous photofragment. As an example, the power dependence of the total fluorescence of the C_2 Swan system is illustrated in Figure 5a. A log−log plot of signal intensity versus laser energy with a slope of 3.0 ± 0.1 is presented in Figure 5b. Similar illustrations for selected photofragments are displayed in Figures 6−8. The power dependence measurements for the major

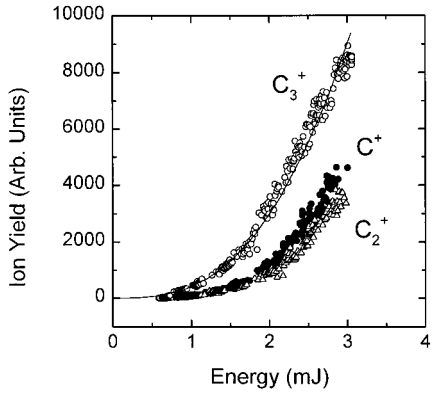

Figure 6. Laser-power dependencies of the C_3^+, C_2^+, and C^+ photofragments. The solid line along C_3^+ results from the simulation with $\sigma = 1.8 \times 10^{-17}$ cm^2 for C_3H_2 at 193 nm excitation.

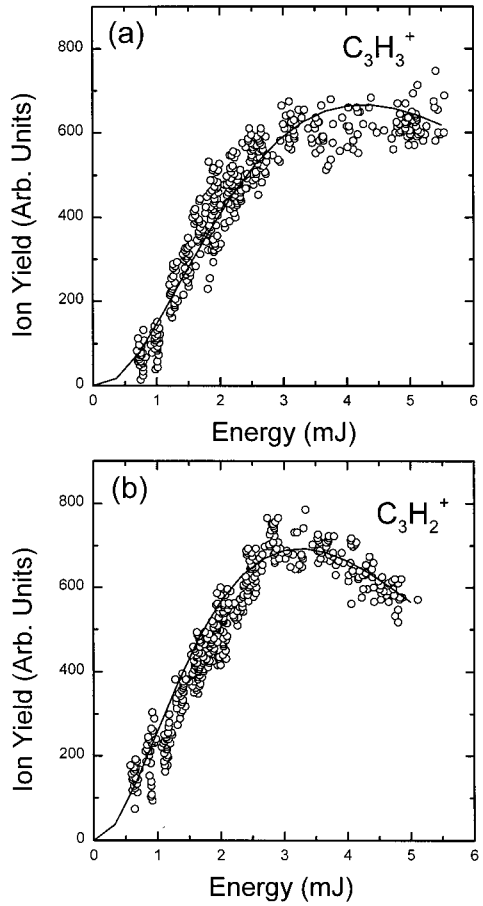

Figure 7. Laser-power dependencies of the $C_3H_3^+$ and $C_3H_2^+$ photofragments. The solid lines result from the simulation with (a) $\sigma(C_3H_3^+) = 5.9 \times 10^{-19}$ cm^2, (b) $\sigma(C_3H_2^+) = 1 \times 10^{-18}$ cm^2, and other parameters listed in Table 2.

photofragments and the slopes from log−log plots of signal intensity versus laser energy are summarized in Table 1. The slopes were analyzed in the relatively low-energy region, where the experimental data fit very closely to a straight line (e.g., Figure 5b).

At the limit of low laser flux, the slope from the power dependence measurement indicates the number of photons needed to yield the corresponding photofragment.[44] This indication is not necessarily true in this experiment, however, because of the possible optical saturation in high energy flux of the focused laser beam. Instead, the measured photon number should be regarded as indicating a lower limit in deducing how many

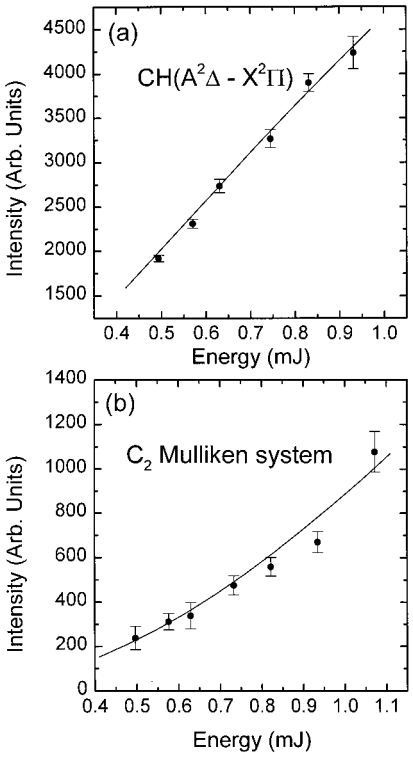

Figure 8. Laser-power dependencies of the $CH(A^2\Delta)$ and $C_2(D^1\Sigma_u^+)$ photofragments. The solid line in (a) results from the simulation with $\sigma = 6 \times 10^{-18}$ cm^2 for C_3H_3 at 193 nm excitation. The solid line in (b) results from the simulation using the same σ value for C_3H_2 in Figure 6.

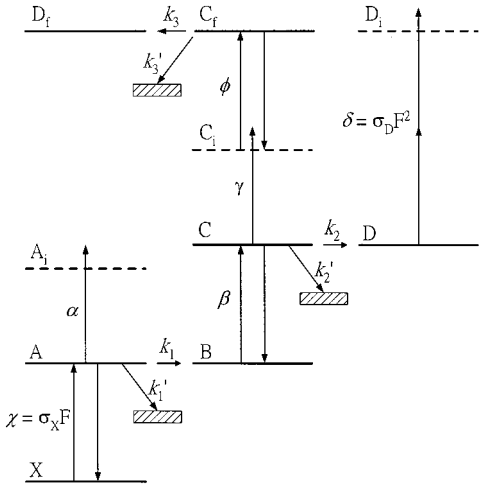

Figure 9. Schematic diagram of the kinetic model (see text).

photons are involved in the reaction processes. In discussing the power dependence of the product yields, a kinetic model including a set of coupled differential equations appropriate for describing the reaction mechanisms will be helpful.[44] This model was built, and we have solved the equations in section 4.1 to illuminate the photodissociation/ionization mechanisms of allene.

4. Discussion

4.1. Kinetic Model. The slope value measured from the power dependence will not follow the I^n law in an n-photon process[44] if the laser flux is beyond the low-flux limit or if other competing channels (e.g., dissociation versus ionization) are involved in the process. In this experiment, the observed

TABLE 1: Major Ionic and Luminous Photofragments Observed in the Photodissociation/Ionization of Allene Excited at 193 nm

photofragment	slope[a]	proposed mechanism[b]	photons needed[c]
C_3^+	2.9 ± 0.1	$C_3H_4 \rightarrow C_3H_2 \dot{\rightarrow} C_3 \Rightarrow C_3^+$	4
C_2^+	3.6 ± 0.1	$C_3H_4 \rightarrow C_3H_2 \dot{\rightarrow} C_3 \Rightarrow C_3^+ \rightarrow C_2^+$	5
C^+	3.9 ± 0.1	$C_3H_4 \rightarrow C_3H_2 \dot{\rightarrow} C_3 \Rightarrow C_3^+ \rightarrow C^+$	5
$CH(A^2\Delta)$	1.3 ± 0.1	$C_3H_4 \rightarrow C_3H_3 \dot{\rightarrow} CH(A)$	2
$C_2(d^3\Pi_g)$	3.0 ± 0.1	$C_3H_4 \rightarrow C_3H_2 \dot{\rightarrow} C_3 \Rightarrow C_2(d)$	4
$C_2(D^1\Sigma_u^+)$	1.9 ± 0.1	$C_3H_4 \rightarrow C_3H_2 \dot{\Rightarrow} C_2(D)$	3
$C(2p3s\ ^1P^o)$	4.2 ± 0.1	$C_3H_4 \rightarrow C_3H_2 \dot{\rightarrow} C_3 \Rightarrow C(^1D) \rightarrow C(^1P^o)$	5

[a] The slopes are measured from laser-power dependence. [b] → and ⇒ symbolizing one- and two-photon excitations, respectively. The dot symbol above the arrow indicates an optical saturation in the corresponding process. [c] The needed photon number based on the proposed mechanisms without optical saturation.

products resulted from the photodissociation and ionization of allene. To interpret the measured laser-power dependence, a kinetic model based on the possible photodissociation/ionization mechanisms of allene is proposed. A schematic diagram of the kinetic model is depicted in Figure 9.

The parent molecule (X) absorbs one photon to reach an excited state (A). Following the excitation, the fragmentation of A with rate constant k_1 can occur to form B or the ionization of A by absorbing one more photon to form A_i. Other decay channels from A, such as internal conversion, intersystem crossing, and fragmentation to form other products, are represented by an effective rate constant, k_1'. As a result of the high power of the short-pulsed laser in the present experiment, only the absorption and stimulated-emission processes were taken into account; the spontaneous emission was neglected because of its relatively slower rate. Herein, the absorption and stimulated-emission rates are assumed to be the same. Similar processes are proposed for the primary fragment B. The excitation of B to C and the ionization and dissociation of C are depicted in Figure 9. The photodissociation of C_i ions generated from the primary fragment B was also considered. The corresponding levels are C_i, C_f and D_f as presented in Figure 9. So far, this model is sufficient to describe the power dependence for all ionic and neutral photofragments generated in the primary and secondary reactions in a usual UV-photolysis experiment. In addition, a two-photon ionization process, for the secondary fragment D was added to the model to specifically account for the $C_3 + 2h\nu_{193nm} \rightarrow C_3^+$ in this experiment, as discussed in section 4.2.1.

Under the laser excitation with homogeneous rectangular pulse duration of τ, the following rate equations for the levels X, A, A_i, and B were set up (Figure 9):

$$\dot{X} = -\chi X + \chi A \tag{1}$$

$$\dot{A} = \chi X - \chi A - (k_1 + k_1' + \alpha)A \tag{2}$$

$$\dot{A}_i = \alpha A \tag{3}$$

$$\dot{B}_0 = k_1 A \tag{4}$$

where X, A, and A_i are the number densities in molecular states X, A, and A_i, respectively. The dots in equations denote the differentiation with respect to time (e.g., $\dot{X} = dX/dt$). B_0 is the initial number density of fragment B generated from A. $\chi = \sigma_X F$ and $\alpha = \sigma_A F$ represent the absorption rates, where F is the laser flux (photons $cm^{-2}\ s^{-1}$) and σ_X and σ_A are absorption cross sections (cm^2) for molecular states X and A, respectively. By this definition, χ, α, k, and k' are all in the unit of s^{-1}.

Equations 1−4 can be solved with the initial conditions of $X(0) = X_0$, $A(0) = A_i(0) = B_0(0) = 0$ (i.e., at the beginning, $t = 0$, only the parent molecules exist with number density X_0.). The solutions are

$$X = \frac{X_0}{r_1 - r_2}[(r_1 - \chi)\, e^{-r_2\tau} - (r_2 - \chi)\, e^{-r_1\tau}] \tag{5}$$

$$A = \frac{\chi X_0}{r_1 - r_2}(e^{-r_2\tau} - e^{-r_1\tau}) \tag{6}$$

$$A_i = \frac{\alpha\chi X_0}{r_1 - r_2}\left(\frac{1 - e^{-r_2\tau}}{r_2} - \frac{1 - e^{-r_1\tau}}{r_1}\right) \tag{7}$$

$$B_0 = \frac{k_1\chi X_0}{r_1 - r_2}\left(\frac{1 - e^{-r_2\tau}}{r_2} - \frac{1 - e^{-r_1\tau}}{r_1}\right) \tag{8}$$

In eqs 5−8,

$$r_1 = \frac{1}{2}[(2\chi + k_1 + k_1' + \alpha) + \sqrt{4\chi^2 + (k_1 + k_1' + \alpha)^2}] \tag{9}$$

and

$$r_2 = \frac{1}{2}[(2\chi + k_1 + k_1' + \alpha) - \sqrt{4\chi^2 + (k_1 + k_1' + \alpha)^2}] \tag{10}$$

Similarly, the rate equations for the primary fragment B can be represented as

$$\dot{B} = k_1 A - \beta B + \beta C \tag{11}$$

$$\dot{C} = \beta B - \beta C - (k_2 + k_2' + \gamma)C \tag{12}$$

$$\dot{C}_{i0} = \gamma C \tag{13}$$

$$\dot{D}_0 = k_2 C \tag{14}$$

where C_{i0} and D_0 are the nascent number densities of the primary ion C_i and the secondary fragment D, respectively. With the initial conditions of $B(0) = C(0) = C_{i0}(0) = D_0(0) = 0$, the solutions are

$$B = \frac{k_1\chi X_0}{s_1 - s_2}\left[\frac{(s_1 - \beta)\, e^{-s_2\tau}}{(r_1 - s_2)(r_2 - s_2)} - \frac{(s_2 - \beta)\, e^{-s_1\tau}}{(r_1 - s_1)(r_2 - s_1)}\right] + \frac{k_1\chi X_0}{r_1 - r_2}\left[\frac{(s_1 + s_2 - \beta - r_2)\, e^{-r_2\tau}}{(s_1 - r_2)(s_2 - r_2)} - \frac{(s_1 + s_2 - \beta - r_1)\, e^{-r_1\tau}}{(s_1 - r_1)(s_2 - r_1)}\right] \tag{15}$$

$$C = \frac{k_1\beta\chi X_0}{s_1 - s_2}\left[\frac{e^{-s_2\tau}}{(r_1 - s_2)(r_2 - s_2)} - \frac{e^{-s_1\tau}}{(r_1 - s_1)(r_2 - s_1)}\right] + \frac{k_1\beta\chi X_0}{r_1 - r_2}\left[\frac{e^{-r_2\tau}}{(s_1 - r_2)(s_2 - r_2)} - \frac{e^{-r_1\tau}}{(s_1 - r_1)(s_2 - r_1)}\right] \quad (16)$$

$$C_{i0} = \frac{k_1\beta\gamma\chi X_0}{s_1 - s_2}\left[\frac{1 - e^{-s_2\tau}}{s_2(r_1 - s_2)(r_2 - s_2)} - \frac{1 - e^{-s_1\tau}}{s_1(r_1 - s_1)(r_2 - s_1)}\right] + \frac{k_1\beta\gamma\chi X_0}{r_1 - r_2}\left[\frac{1 - e^{-r_2\tau}}{r_2(s_1 - r_2)(s_2 - r_2)} - \frac{1 - e^{-r_1\tau}}{r_1(s_1 - r_1)(s_2 - r_1)}\right] \quad (17)$$

$$D_0 = \frac{k_1k_2\beta\chi X_0}{s_1 - s_2}\left[\frac{1 - e^{-s_2\tau}}{s_2(r_1 - s_2)(r_2 - s_2)} - \frac{1 - e^{-s_1\tau}}{s_1(r_1 - s_1)(r_2 - s_1)}\right] + \frac{k_1k_2\beta\chi X_0}{r_1 - r_2}\left[\frac{1 - e^{-r_2\tau}}{r_2(r_2 - s_1)(r_2 - s_2)} - \frac{1 - e^{-r_1\tau}}{r_1(r_1 - s_1)(r_1 - s_2)}\right] \quad (18)$$

where

$$s_1 = \frac{1}{2}[(2\beta + k_2 + k_2' + \gamma) + \sqrt{4\beta^2 + (k_2 + k_2' + \gamma)^2}] \quad (19)$$

and

$$s_2 = \frac{1}{2}[(2\beta + k_2 + k_2' + \gamma) - \sqrt{4\beta^2 + (k_2 + k_2' + \gamma)^2}] \quad (20)$$

If the photofragment D is ionized with a two-photon excitation (Figure 9), the rate equations for D and D_i can be written as

$$\dot{D} = k_2C - \delta D \quad (21)$$

and

$$\dot{D} = \delta D \quad (22)$$

With the initial conditions of $D(0) = D_i(0) = 0$, the solutions are

$$D = k_1k_2\beta\chi X_0\left[\frac{e^{-\delta\tau}}{(r_1 - \delta)(r_2 - \delta)(s_1 - \delta)(s_2 - \delta)}\right] + \frac{k_1k_2\beta\chi X_0}{s_1 - s_2}\left[\frac{e^{-s_2\tau}}{(\delta - s_2)(r_1 - s_2)(r_2 - s_2)} - \frac{e^{-s_1\tau}}{(\delta - s_1)(r_1 - s_1)(r_2 - s_1)}\right] + \frac{k_1k_2\beta\chi X_0}{r_1 - r_2}\left[\frac{e^{-r_2\tau}}{(\delta - r_2)(s_1 - r_2)(s_2 - r_2)} - \frac{e^{-r_1\tau}}{(\delta - r_1)(s_1 - r_1)(s_2 - r_1)}\right] \quad (23)$$

$$D_i = k_1k_2\beta\chi X_0\left[\frac{1 - e^{-\delta\tau}}{(r_1 - \delta)(r_2 - \delta)(s_1 - \delta)(s_2 - \delta)}\right] + \frac{k_1k_2\beta\delta\chi X_0}{s_1 - s_2}\left[\frac{1 - e^{-s_2\tau}}{s_2(\delta - s_2)(r_1 - s_2)(r_2 - s_2)} - \frac{1 - e^{-s_1\tau}}{s_1(\delta - s_1)(r_1 - s_1)(r_2 - s_1)}\right] + \frac{k_1k_2\beta\delta\chi X_0}{r_1 - r_2}\left[\frac{1 - e^{-r_2\tau}}{r_2(\delta - r_2)(s_1 - r_2)(s_2 - r_2)} - \frac{1 - e^{-r_1\tau}}{r_1(\delta - r_1)(s_1 - r_1)(s_2 - r_1)}\right] \quad (24)$$

For the subsequent photodissociation from C_i (Figure 9), we have

$$\dot{C}_i = \gamma C - \phi C_i + \phi C_f \quad (25)$$

$$\dot{C}_f = \phi C_i - \phi C_f + (k_3 + k_3')C_f \quad (26)$$

$$\dot{D}_f = k_3C_f \quad (27)$$

With the initial conditions of $C_i(0) = C_f(0) = D_f(0) = 0$, the solutions are

$$C_i = \frac{k_1\beta\gamma\chi X_0}{u_1 - u_2}\left[\frac{(u_1 - \phi)\,e^{-u_2\tau}}{(r_1 - u_2)(r_2 - u_2)(s_1 - u_2)(s_2 - u_2)} - \frac{(u_2 - \phi)\,e^{-u_1\tau}}{(r_1 - u_1)(r_2 - u_1)(s_1 - u_1)(s_2 - u_1)}\right] + \frac{k_1\beta\gamma\chi X_0}{s_1 - s_2}\left[\frac{(u_1 + u_2 - \phi - s_2)\,e^{-s_2\tau}}{(r_1 - s_2)(r_2 - s_2)(u_1 - s_2)(u_2 - s_2)} - \frac{(u_1 + u_2 - \phi - s_1)\,e^{-s_1\tau}}{(r_1 - s_1)(r_2 - s_1)(u_1 - s_1)(u_2 - s_1)}\right] + \frac{k_1\beta\gamma\chi X_0}{r_1 - r_2}\left[\frac{(u_1 + u_2 - \phi - r_2)\,e^{-r_2\tau}}{(s_1 - r_2)(s_2 - r_2)(u_1 - r_2)(u_2 - r_2)} - \frac{(u_1 + u_2 - \phi - r_1)\,e^{-r_1\tau}}{(s_1 - r_1)(s_2 - r_1)(u_1 - r_1)(u_2 - r_1)}\right] \quad (28)$$

$$C_f = \frac{k_1\beta\gamma\phi\chi X_0}{u_1 - u_2}\left[\frac{e^{-u_2\tau}}{(r_1 - u_2)(r_2 - u_2)(s_1 - u_2)(s_2 - u_2)} - \frac{e^{-u_1\tau}}{(r_1 - u_1)(r_2 - u_1)(s_1 - u_1)(s_2 - u_1)}\right] + \frac{k_1\beta\gamma\phi\chi X_0}{s_1 - s_2}\left[\frac{e^{-s_2\tau}}{(r_1 - s_2)(r_2 - s_2)(u_1 - s_2)(u_2 - s_2)} - \frac{e^{-s_1\tau}}{(r_1 - s_1)(r_2 - s_1)(u_1 - s_1)(u_2 - s_1)}\right] + \frac{k_1\beta\gamma\phi\chi X_0}{r_1 - r_2}\left[\frac{e^{-r_2\tau}}{(s_1 - r_2)(s_2 - r_2)(u_1 - r_2)(u_2 - r_2)} - \frac{e^{-r_1\tau}}{(s_1 - r_1)(s_2 - r_1)(u_1 - r_1)(u_2 - r_1)}\right] \quad (29)$$

$$D_f = \frac{k_1 k_3 \beta\gamma\phi\chi X_0}{u_1 - u_2}\left[\frac{1 - e^{-u_2\tau}}{u_2(r_1 - u_2)(r_2 - u_2)(s_1 - u_2)(s_2 - u_2)} - \frac{1 - e^{-u_1\tau}}{u_1(r_1 - u_1)(r_2 - u_1)(s_1 - u_1)(s_2 - u_1)}\right] + \frac{k_1 k_3 \beta\gamma\phi\chi X_0}{s_1 - s_2}\left[\frac{1 - e^{-s_2\tau}}{s_2(r_1 - s_2)(r_2 - s_2)(u_1 - s_2)(u_2 - s_2)} - \frac{1 - e^{-s_1\tau}}{s_1(r_1 - s_1)(r_2 - s_1)(u_1 - s_1)(u_2 - s_1)}\right] + \frac{k_1 k_3 \beta\gamma\phi\chi X_0}{r_1 - r_2}\left[\frac{1 - e^{-r_2\tau}}{r_2(s_1 - r_2)(s_2 - r_2)(u_1 - r_2)(u_2 - r_2)} - \frac{1 - e^{-r_1\tau}}{r_1(s_1 - r_1)(s_2 - r_1)(u_1 - r_1)(u_2 - r_1)}\right] \quad (30)$$

where

$$u_1 = \frac{1}{2}[(2\phi + k_3 + k_3') + \sqrt{4\phi^2 + (k_3 + k_3')^2}] \quad (31)$$

and

$$u_2 = \frac{1}{2}[(2\phi + k_3 + k_3') - \sqrt{4\phi^2 + (k_3 + k_3')^2}] \quad (32)$$

In the preceding equations, χ, α, β, γ, δ, and ϕ are associated with laser flux and absorption cross sections. The laser pulse duration (τ), laser flux, and the number density of parent molecules (X_0) are derived from the experimental condition. If the absorption cross sections and rate constants (k and k') are known, the yield of each photofragment relating to the applied laser energy can be calculated from the preceding equations. In case only partial parameters are known, computer simulation for the kinetic model, in comparison to experimental data, can still provide qualitative information concerning branching reactions.

To apply the kinetic model to the photodissociation/ionization of allene (C_3H_4), we set X = C_3H_4, A_i = $C_3H_4^+$, B = C_3H_3 or C_3H_2, C_i = $C_3H_3^+$ or $C_3H_2^+$. Level A may correspond to the S_1 or S_2 electronic state of C_3H_4, as discussed by Jackson et al.[35] The primary photofragment is either C_3H_3 or C_3H_2, on the basis of the observation by Jackson et al.[32] and Sun et al.[33] Level C can be an excited electronic state of C_3H_3 or C_3H_2. According to Jackson et al.,[32] the secondary photodissociation of allene with the primary photofragment of C_3H_3 can lead to C_3H_2 + H, C_3H + H_2, and C_2H_2 + CH. The secondary photodissociation of allene via C_3H_2 results in C_3 + H_2, C_2H + CH, and C_2H_2 + C. Any of these photofragments can be defined as D in this model. As mentioned earlier, D_i is specifically designed to represent the most abundant ionic fragment of C_3^+ in this study, which comes from C_3 with a two-photon excitation as will be discussed in section 4.2.1.

4.2. Photodissociation and Ionization Mechanisms. This section proposes the photodissociation/ionization mechanisms of allene that lead to the formation of the observed ionic and luminous products. The feasibility of the proposed photodissociation/ionization processes is decided exclusively from the thermodynamic point of view. In other words, the proposed reaction processes were selected without considering activation energy. The multiphoton energy available in the reactions was determined from the power-dependence experiments. For example, the measured power dependence of the $C_2(d^3\Pi_g)$ state indicates that at least three photons are involved in the reaction. The study examines the possible reaction channels for C_3H_4 leading to the simultaneous or sequential formation of $C_2(d^3\Pi_g)$ with three-photon excitation. If no appropriate reaction channels can be suggested under the constraint of three-photon steps, the study seeks a four-photon excitation on the assumption that there is an optical saturation in a particular process. The assumption is examined later by simulating laser-power dependence using the kinetic model derived in section 4.1.

4.2.1. C_3^+. The possible precursors for the most abundant ionic product, C_3^+, in the photodissociation/ionization of C_3H_4 are

$$C_3 \rightarrow C_3^+ + e^-, \quad \Delta H = 12.0 \text{ eV} \quad (33)$$

$$C_3H \rightarrow C_3^+ + H + e^-, \quad \Delta H = 14.11 \text{ eV} \quad (34)$$

$$C_3H_2 \rightarrow C_3^+ + H_2 + e^-, \quad \Delta H = 14.59 \text{ eV} \quad (35)$$

$$C_3H_3 \rightarrow C_3^+ + H_2 + H + e^-, \quad \Delta H = 18.77 \text{ eV} \quad (36)$$

and

$$C_3H_4 \rightarrow C_3^+ + 2H_2 + e^-, \quad \Delta H = 18.2 \text{ eV} \quad (37)$$

ΔH's are calculated from the energies of the neutral species and the experimental ionization potential of C_3. The energies of the neutral species are adopted from the ab initio values reported by Mebel et al.[36] The adiabatic ionization potential of C_3 is less certain. Rohlfing et al. measured the ionization potential of C_3 (9.98−11.61 eV) using the photoionization of carbon clusters with TOF mass analysis.[45] Ramanathan et al. have determined the ionization potential of C_3 (12.97 ± 0.1 eV) through the use of charge-transfer methods.[46] However, Lemire et al. reported an upper limit (12.0 eV) for the adiabatic ionization potential of C_3 from resonant ionization spectra of jet-cooled C_3.[47] This study takes the value of 12.0 eV for analysis.

Examining the precursors in eqs 34−37, at least three photons (193 nm ≈ 6.42 eV) are needed to produce C_3^+ from C_3H_n (n = 1−4). However, any two-photon excitation of C_3H_n in this experiment can lead to the formation of $C_3H_n^+$ [IP(C_3H_4) = 9.69 eV,[48] IP(C_3H_3) = 8.67 eV,[49] IP(C_3H_2) = 10.43 eV,[29] IP(C_3H) = 9.06 eV[15]]. According to the electron-impact ionization mass spectrum of allene,[50] the relative abundance of the ionic fragments is $C_3H_4^+/C_3H_3^+/C_3H_2^+/C_3H^+$ = 100.0/89.6/34.4/27.0, where the $C_3H_n^+$ ions are considerably stable under the collisionless condition in a vacuum. In view of the weak $C_3H_n^+$ and strong C_3^+ signals in the present experiment (Figure 2), C_3H_n is unlikely to be the precursor of C_3^+. Instead, C_3^+ is likely to be ionized from C_3 with a two-photon excitation as represented in eq 33.

Song et al. measured the internal-state population distribution of C_3 from the photolysis of allene at 193 nm.[34] According to their results, C_3 is populated in the (0, 0, 0) and (0, 1, 0) vibrational states of the ground electronic potential. Jackson and co-workers proposed the mechanism for producing C_3 as expressed in the following:[34,35]

$$C_3H_4 \rightarrow C_3H_2 + H_2, \quad \Delta H = 3.60 \text{ eV} \quad (38)$$

and

$$C_3H_2 \rightarrow C_3 + H_2, \quad \Delta H = 2.59 \text{ eV} \quad (39)$$

On the basis of this mechanism and the argument that C_3^+ is ionized from C_3, the conclusion is that C_3^+ resulted from the

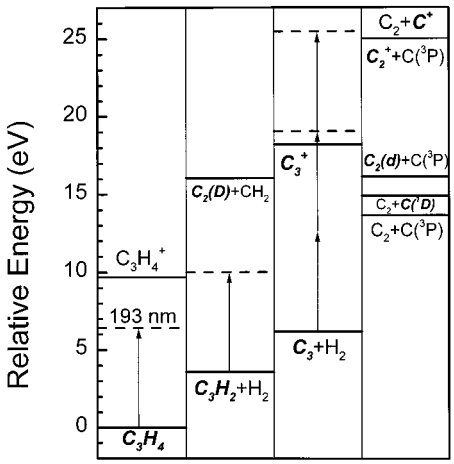

Figure 10. Energy diagram for the reaction channels from C_3H_4 via C_3H_2. Arrows are used to scale a single-photon energy at 193 nm. Chemical species are located at their ground states unless otherwise specified.

photodissociation/ionization of C_3H_4 via the channels of eqs 38, 39, and 33, requiring four photons in the processes (Figure 10).

Nevertheless, the power-dependence measurement of C_3^+ indicates a slope of 2.9, which is approximately one unit less than proposed (Table 1). Although the (one-photon) absorption cross sections of C_3H_2 and C_3 at 193 nm have not yet been measured, 6×10^{-19} cm^2 has been determined for allene.[31] With this cross section and the laser flux used in this experiment, optical saturation should not occur for allene in eq 38. As estimated, the two-photon absorption cross section for C_3 at 193 nm is $10^{-48}-10^{-54}$ cm^4 s as is usual for most molecules.[51] Under this estimation, saturation could not occur for C_3 in eq 33 either. Alternatively, saturation may occur in eq 39; i.e., the (one-photon) absorption cross section of C_3H_2 at 193 nm is large. Despite lacking the absorption value at 193 nm, the matrix-isolation spectra for different C_3H_2 isomers have all shown strong vibronic transitions around 200 nm.[28] The saturation can be further rationalized through the use of a computer simulation (eq 24) of the power dependence of C_3^+, following the mechanisms of eqs 38, 39, and 33.

In our simulation, X_0 is used as an adjusting parameter and the dissociations in eqs 38 and 39 are assumed to take place on the order of $1-10^3$ picoseconds (i.e., rate constants $= 10^9-10^{12}$ s^{-1}). The ionization cross sections for the electronically excited C_3H_4 and C_3H_2 are assumed to be small ($\sim 6 \times 10^{-21}$ cm^2), in accordance with the low yields of $C_3H_4^+$ and $C_3H_2^+$ observed in this experiment. The simulation result, as illustrated in Figure 6 by the solid line along C_3^+, closely corresponds to the experimental data, when the absorption cross section of C_3H_2 at 193 nm is set to be larger than 1.8×10^{-17} cm^2! This agreement is rewarding and suggests that the optical saturation in ref 39 indeed exists under the present experimental conditions. The numerical values for the absorption cross sections and dissociation rate constants used in the simulation are listed in Table 2. Owing to lack of information about the photodissociation/ionization of allene, many absorption cross sections and dissociation rates in the mechanisms are unknown. The simulations throughout this study have been obtained mainly as "orders of magnitude" for the parameters, as listed in Table 2.

4.2.2. C_2^+, C^+. The laser-power dependencies of C_2^+ and C^+ are displayed in Figure 6. The rising behavior of C_2^+ and C^+ presented in Figure 6 are very similar in the low-flux region, indicating that they might be produced simultaneously from the same precursor, C_3^+. The ionization potentials for C_2 and C are 11.35 [11] and 11.26 eV,[41] respectively. The heats of formation of C_2^+ and C^+ from C_3^+ are

$$C_3^+ \rightarrow C_2^+ + C, \quad \Delta H = 6.81 \text{ eV} \tag{40}$$

and

$$C_3^+ \rightarrow C_2 + C^+, \quad \Delta H = 6.78 \text{ eV} \tag{41}$$

The energy corresponding to a single photon at 193 nm (6.42 eV) is not enough to make possible the reactions in eqs 40 and 41 if the C_3^+ ions are populated in the ground state. However, if the internal energy of C_3^+ exceeds 0.4 eV, both reaction channels are energetically feasible. In the two-photon ionization of C_3 at 193 nm, at least 0.84 eV is left over. The leftover energy can be deposited to the ejected electron or the ionized C_3^+. In the latter energy deposition, C_3^+ is likely to gain its internal energy and thus make the reactions in eqs 40 and 41 possible.

The slopes of C_2^+ and C^+ in the power-dependence measurements are approximately one unit more than that of C_3^+ (Table 1), consistent with the proposed mechanism that C_2^+ and C^+ are generated from the one-photon excitation of internally hot C_3^+ (Figure 10). The difference in the slopes of C_2^+ (3.6 ± 0.1) and C^+ (3.9 ± 0.1), especially at higher laser flux (Figure 6), may be attributed to further fragmentation of C_2^+ (i.e., $C_2^+ \rightarrow C + C^+$) in the high-flux region.

4.2.3. $C_3H_n^+$ ($n = 1-4$). The laser-power dependencies of $C_3H_3^+$ and $C_3H_2^+$ are presented in Figure 7. The $C_3H_3^+$ and $C_3H_2^+$ signals are more easily saturated than C_n^+ ($n = 1-3$) (Figure 6) under the present experimental condition. At a laser energy of $\sim$3 mJ, the $C_3H_3^+$ signal intensity becomes saturated, but $C_3H_2^+$ begins to decrease. This clearly suggests a larger absorption cross section for $C_3H_2^+$ than for $C_3H_3^+$ at 193 nm. The larger cross section may trigger other reactions in $C_3H_2^+$, resulting in the depletion of its population. The laser-power dependence of C_3H^+ closely resembles that of $C_3H_3^+$ (Figure 7a), except that it becomes saturated at a slightly higher energy level ($\sim$3.5 mJ).

This study simulated the laser-power dependencies of $C_3H_3^+$ and $C_3H_2^+$ by using eq 28, where the photodissociations of $C_3H_3^+$ and $C_3H_2^+$ have been included. The solid lines along the experimental data points in Figure 7 denote the simulation results. The correlation is good when $\sigma(C_3H_3^+) = 5.9 \times 10^{-19}$ cm^2 and $\sigma(C_3H_2^+) = 1.0 \times 10^{-18}$ cm^2 are assumed (Table 2). The absorption cross section for $C_3H_2^+$ at 193 nm is indeed greater than that for $C_3H_3^+$, as mentioned earlier.

The yields of $C_3H_n^+$ ($n = 1-3$) are relatively low (Figure 2). The signal of $C_3H_4^+$ is even smaller. In contrast, the relative abundance in the electron-impact ionization of allene[50] is $C_3H_4^+/C_3H_3^+/C_3H_2^+/C_3H^+ = 100.0/89.6/34.4/27.0$, in which the parent ion is most abundant. The distinctively different experimental results between the laser-induced dissociation/ionization at 193 nm and the electron-impact ionization reveal that the dissociation of C_3H_n ($n = 1-4$) is more favorable in competing against the multiphoton ionization process within the laser energy used in this experiment.

The lack of $C_3H_4^+$ signal in the two-photon ionization of C_3H_4 could be due to (a) extremely weak transition moment, (b) fast dissociation in the intermediate state, or (c) fast fragmentation of $C_3H_4^+$. The simulation discovered that $\alpha < 10^6$ s^{-1} (Figure 9), which is much smaller than the dissociation rates of the excited C_3H_4 (10^9-10^{12} s^{-1}). Therefore, both (a) and (b) appropriately account for the very weak $C_3H_4^+$ signal. Although the appearance potential of $C_3H_3^+$ determined from the photoionization of allene is 12.27 eV,[50] which suggests that the

TABLE 2: Absorption Cross Sections and Dissociation Rate Constants Used in Simulation

parameter[a]	$C_3H_3^+$ [b]	$CH(A^2\Delta)$[b]	$C_3H_2^+$ [c]	C_3^+ [c]	$C_2(D^1\Sigma_u^+)$[c]
σ(B)	6×10^{-18}	6×10^{-18}	1.8×10^{-17}	1.8×10^{-17}	1.8×10^{-17}
$\sigma(C_i)$	5.9×10^{-19}		1×10^{-18}		
σ(D)				1×10^{-48}	
k_1	5×10^{11}	5×10^{11}	1×10^{11}	1×10^{11}	1×10^{11}
k_1'	1×10^{11}	1×10^{11}	5×10^{11}	5×10^{11}	5×10^{11}
k_3	1×10^{11}		1×10^{11}		

[a] For each photofragment, $\sigma(X) = 6 \times 10^{-19}$, $\sigma(A) = \sigma(C) = 6 \times 10^{-21}$, $k_2 = k_2'/5 = 1 \times 10^{11}$, and $k_3' = 0$. The units for σ and k are cm^2 and s^{-1}, respectively. [b] The primary photofragment is C_3H_3. [c] The primary photofragment is C_3H_2.

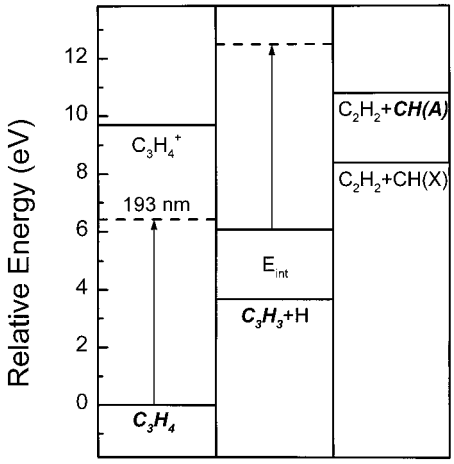

Figure 11. Energy diagram for the reaction channels from C_3H_4 via C_3H_3.

reactions of $C_3H_4 + 2h\nu_{193nm} \rightarrow C_3H_4^+ \rightarrow C_3H_3^+ + H$ are energetically feasible, the fast fragmentation of $C_3H_4^+$ under the collisionless condition in a vacuum seems less probable, as discussed in section 4.2.1.

4.2.4. $CH(A^2\Delta)$. In the primary photodissociation of allene at 193 nm measured using translational spectroscopy, Jackson et al. observed that the internal energy distribution of C_3H_3 peaked at 2.4 eV.[32] Energetically, the formation of $CH(A^2\Delta)$ can be realized with two-photon (193 nm) excitation of allene via the internally hot C_3H_3 of 2.4 eV, as follows.

$$C_3H_4 \rightarrow C_3H_3 + H, \quad \Delta H = 3.81 \text{ eV} \qquad (42)$$

and

$$C_3H_3 \rightarrow C_2H_2 + CH(A^2\Delta), \quad \Delta H = 7.12 \text{ eV} \qquad (43)$$

The large amount of internal energy in C_3H_3 makes the formation of CH at $X^2\Pi$ or $A^2\Delta$ via eq 43 energetically possible (Figure 11). For CH ($A^2\Delta$), the slope of 1.3 in the power-dependence measurement, rather than 2 expected from eqs 42 and 43, could be a consequence of partial saturation in eq 43. This would further suggest that the absorption cross section (at 193 nm) of internally hot C_3H_3 is larger than 6×10^{-19} cm^2 of allene. This suggestion is indirectly supported by a recent measurement[52] that the propargyl radical (C_3H_3) has an absorption cross section of 1.2×10^{-17} cm^2 at 242 nm ($\pi^* \leftarrow \pi$), and several other $\pi^* \leftarrow \pi$ and $\pi^* \leftarrow$ p transitions are calculated to be located in the spectral range 120−200 nm. The partial saturation has also been examined by comparing the experimental data with a simulation using eq 18. A good agreement is achieved (Figure 8a) when the absorption cross section of C_3H_3 is set to be larger than 6×10^{-18} cm^2 (Table 2). This agreement also confirms the optical saturation in eq 43 under the present experimental condition.

4.2.5. $C_2(d^3\Pi_g)$ Swan System. The C_2 Swan system, $C_2(d^3\Pi_g)$, is of importance in combustion, atmospheric chemistry, and astrophysics; it has been observed in the photolysis of many hydrocarbons.[42] However, this is the first study to demonstrate that allene is also a source of C_2 Swan system, by irradiating 193 nm light. The slope in the power-dependence measurement for C_2 Swan system is 3.0, which is close to that of C_3^+ (Table 1). This study proposes that $C_2(d^3\Pi_g)$ is generated from the photodissociation of C_3 with a two-photon excitation (Figure 10).

$$C_3 \rightarrow C_2(d^3\Pi_g) + C, \quad \Delta H = 9.84 \text{ eV} \qquad (44)$$

The C_3, as mentioned earlier, comes from eqs 38 and 39. Again, following the aforementioned saturation in eq 39, the generation of C_2 Swan system from C_3H_4 needs only three photons, consistent with the measured slope value. The highly vibrational excitation in the $C_2(d^3\Pi_g)$ state, as illustrated in Figure 3b, probably resulted from an impulsive breaking of one of the carbon−carbon bonds of C_3 leading to a nonthermal population distribution (Figure 4).

4.2.6. $C_2(D^1\Sigma_u^+)$ Mulliken System. The slope in the power-dependence measurement for the $C_2(D^1\Sigma_u^+)$ Mulliken system is 1.9, in contrast to 3.0 for the $C_2(d^3\Pi_g)$ Swan system (Table 1). Moreover, $C_2(D^1\Sigma_u^+)$ is ~3 eV higher than $C_2(d^3\Pi_g)$,[40] indicating that the two electronic states of C_2 are produced from different channels. The production of the $C_2(D^1\Sigma_u^+)$ states are proposed to be via C_3H_2 as

$$C_3H_4 \rightarrow C_3H_2 + H_2, \quad \Delta H = 3.60 \text{ eV} \qquad (38)$$

and

$$C_3H_2 \rightarrow CH_2 + C_2(D^1\Sigma_u^+), \quad \Delta H = 12.46 \text{ eV} \qquad (45)$$

In the processes of eqs 38 and 45, three photons are required for generating $C_2(D^1\Sigma_u^+)$ from C_3H_4, as depicted in Figure 10. Similar to eq 39, optical saturation in eq 45 is also assumed when C_3H_2 is excited at 193 nm. This assumption makes understandable the measured slope of 1.9 for $C_2(D^1\Sigma_u^+)$ via eqs 38 and 45. Meanwhile, the same absorption cross section of C_3H_2 (Table 2) has been applied, as was used in eq 39 of section 4.2.1, to simulate the power dependence of the C_2 Mulliken system using eq 17. The solid line in Figure 8b agrees fairly well with the experimental data.

4.2.7. $C(2p3s\ ^1P^o) \rightarrow C(2p^2\ ^1S)$. In this experiment, the narrow dispersed-emission line observed at 247.9 nm has been assigned to be the transition of $C(2p3s\ ^1P^o) \rightarrow C(2p^2\ ^1S)$ in the carbon atom. The corresponding energy levels of the C atom are illustrated in Figure 12.[41] The $C(2p3s\ ^1P^o)$ state promotes an electron from 2p to 3s in nature. The observed atomic line at 247.9 nm is a consequence of the laser-induced fluorescence of $C(2p3s\ ^1P^o) \rightarrow C(2p^2\ ^1S)$ with $C(2p^2\ ^1D)$ being excited by the 193 nm laser at a coincidental resonance. The mechanism

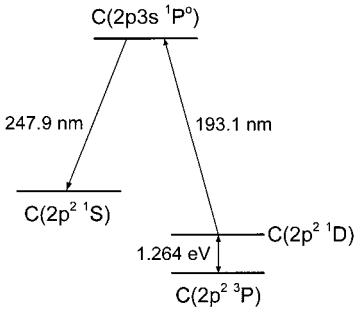

Figure 12. Energy level diagram for the carbon atom.

of $C(2^1D) \xrightarrow{193nm} C(3^1P^o) \xrightarrow{247.9nm} C(2^1S)$ has been studied previously in the photodissociation of CO at 193 nm.[53−58]

From the energy viewpoint, the C(2p^2 ^{1}D) state can be produced from the two-photon excitation of C_3 (Figure 10), i.e.,

$$C_3 \rightarrow C_2 + C(2p^2\ ^1D), \quad \Delta H = 8.72\ \text{eV} \qquad (46)$$

Following the processes in eqs 46, 38, and 39, the measured power-dependence slope of 4.2 for C(2p3s $^1P^o$) is understandable to be one unit less than expected. The short counting of one photon, again, is due to the partial saturation in eq 39.

4.3. Survey of Photodissociation/Ionization Mechanisms. The mechanisms for the formation of ionic and luminous products observed in the photodissociation/ionization of allene in this experiment are summarized in Table 1. The absorption cross sections and dissociation rate constants used in the kinetic model to simulate the laser-power dependence are summarized in Table 2. It is generally true that the parameters used in the simulation in this study fit well when the dissociation rates of C_3H_n dominate the competing ionization rates by 2 or 3 orders of magnitude. The energy diagrams for the possible reaction channels discussed in section 4.2 are depicted in Figures 10 and 11. According to Table 1, the total number of photons needed for each proposed mechanism is approximately one unit more than the experimental measurement. By assuming that C_3H_2 and C_3H_3 are optically saturated in the 193 nm excitation under the present experimental condition, the power-dependence measurements can be nicely accounted for by the proposed mechanisms. The saturation has been supported by some previous reports[28,52] and was further confirmed by simulation using the kinetic model in this study.

The major ionic products are C_n^+ ($n = 1-3$), indicating that the photodissociation of C_3H_n ($n = 1-4$) at 193 nm, with atomic/molecular hydrogen elimination or carbon−carbon bond rupture, is more favorable than the competing multiphoton ionization process in these C_3H_n hydrocarbons. On the other hand, both photodissociation and multiphoton ionization should be possible for C_3 at 193 nm excitation. The (one-photon) absorption cross section for C_3 at 193 nm must be small, which can be justified by the lack of electronic absorption near 193 nm that has been reported in previous investigations on this well-studied molecule.[11] The focused 193 nm laser light thus could cause a two-photon ionization in $C_3 \rightarrow C_3^+$. Alternatively, the two-photon excitation of C_3 at 193 nm could also lead to the photodissociation of $C_3 \rightarrow C_2 + C$ ($\Delta H = 7.46$ eV), as discussed in sections 4.2.5 and 4.2.7. In view of the strong signals in C_3^+ and C_2 observed in this experiment, photodissociation and multiphoton ionization are both feasible for C_3 at 193 nm excitation.

5. Conclusions

This study has detected the ionic and luminous photofragments of allene excited with a focused laser beam at 193 nm. A kinetic model is developed to interpret the laser-power dependence in generating these photofragments in multiphoton processes. In the reaction mechanisms, competition between photodissociation and ionization is discussed. The vibrational population in the $C_2(d^3\Pi_g)$ state is found to be inverted to a thermal equilibrium distribution. This study raises an interesting question. What kind of potential energy surfaces in the dissociative C_3 will lead to the formation of the vibrationally excited $C_2(d^3\Pi_g)$ state in the photodissociation of allene? To answer this question, more experimental and theoretical studies are needed in the future to gain insight into the related reaction dynamics.

Confirmation of the large absorption cross sections of C_3H_3 and C_3H_2 at 193 nm must await additional spectroscopic studies of these molecules. High-resolution laser spectroscopic studies of C_3H_3 and C_3H_2 for the electronic excitation energies and absorption cross sections would be very helpful in examining the proposed saturation in the reaction mechanisms. Rotationally resolved vibronic spectra of C_3H_3 and C_3H_2 would enable definite geometry determination. Isomerization processes among the possible isomers of these floppy molecules, in light of high-resolution laser spectroscopic observation, would be of great importance in studying reaction dynamics.

Acknowledgment. This work is supported by the National Science Council of ROC (NSC-88-2113-M-001-031) and the China Petroleum Corporation. We thank Dr. A. M. Mebel for his comments and fruitful discussion.

References and Notes

(1) Miller, J. A.; Melius, C. F. *Combust. Flame* **1992**, *91*, 21.
(2) Miller, J. A.; Volponi, J. V.; Pauwels, J.-F. *Combust. Flame* **1996**, *105*, 451.
(3) McEnally, C. S.; Pfefferle, L. D. *Combust. Flame* **1998**, *112*, 545.
(4) Thaddeus, P.; Gottlieb, C. A.; Hjalmarson, Å.; Johansson, L. E. B.; Irvine, W. M.; Friberg, P.; Linke, R. A. *Astrophys. J.* **1985**, *294*, L49.
(5) Yamamoto, S.; Saito, S.; Ohishi, M.; Suzuki, H.; Ishikawa, S.-I.; Kaifu, N.; Murakami, A. *Astrophys. J.* **1987**, *322*, L55.
(6) Gottlieb, C. A.; Vrtilek, J. M.; Gottlieb, E. W.; Thaddeus, P.; Hjalmarson, Å. *Astrophys. J.* **1985**, *294*, L55.
(7) Thaddeus, P.; Vrtilek, J. M.; Gottlieb, C. A. *Astrophys. J.* **1985**, *299*, L63.
(8) Matthews, H. E.; Irvine, W. M. *Astrophys. J.* **1985**, *298*, L61.
(9) Cernicharo, J.; Gottlieb, C. A.; Guélin, M.; Killian, T. C.; Paubert, G.; Thaddeus, P.; Vrtilek, J. M. *Astrophys. J.* **1991**, *368*, L39.
(10) Maluendes, S. A.; McLean, A. D.; Herbst, E. *Astrophys. J.* **1993**, *417*, 181.
(11) Weltner, W., Jr.; Van Zee, R. J. *Chem. Rev.* **1989**, *89*, 1713.
(12) Yoshimine, M.; Pacansky, J.; Honjou, N. *J. Am. Chem. Soc.* **1989**, *111*, 4198.
(13) Yoshimine, M.; Pacansky, J.; Honjou, N. *J. Am. Chem. Soc.* **1989**, *111*, 2785.
(14) Honjou, N.; Pacansky, J.; Yoshimine, M. *J. Am. Chem. Soc.* **1985**, *107*, 5332.
(15) Ikuta, S. *J. Chem. Phys.* **1997**, *106*, 4536.
(16) Ochsenfeld, C.; Kaiser, R. I.; Lee, Y. T.; Suits, A. G. *J. Chem. Phys.* **1997**, *106*, 4141.
(17) Takahashi, J.; Yamashita, K. *J. Chem. Phys.* **1996**, *104*, 6613.
(18) Jonas, V.; Böhme, M.; Frenking, G. *J. Phys. Chem.* **1992**, *96*, 1640.
(19) Kiefer, J. H.; Mudipalli, P. S.; Sidhu, S. S.; Kern, R. D.; Jursic, B. S.; Xie, K.; Chen, H. *J. Phys. Chem. A* **1997**, *101*, 4057.
(20) Bettinger, H. F.; Schreiner, P. R.; Schleyer, P. v. R.; Schaefer, H. F., III. *J. Phys. Chem.* **1996**, *100*, 16147.
(21) Seburg, R. A.; McMahon, R. J. *Angew. Chem., Int. Ed. Engl.* **1995**, *34*, 2009.
(22) Tanaka, K.; Sumiyoshi, Y.; Ohshima, Y.; Endo, Y.; Kawaguchi, K. *J. Chem. Phys.* **1997**, *107*, 2728.
(23) Jiang, Q.; Rittby, C. M. L.; Graham, W. R. M. *J. Chem. Phys.* **1993**, *99*, 3194.
(24) Gottlieb, C. A.; Killian, T. C.; Thaddeus, P.; Botschwina, P.; Flügge, J.; Oswald, M. *J. Chem. Phys.* **1993**, *98*, 4478.
(25) Hirota, E.; Matsumura, C. *J. Chem. Phys.* **1973**, *59*, 3038.
(26) Hegelund, F.; Bürger, H.; Polanz, O. *J. Mol. Spectrosc.* **1996**, *175*, 142.

(27) Talbi, D.; Pauzat, F. *Chem. Phys. Lett.* **1995**, *244*, 269.
(28) Seburg, R. A.; Patterson, E. V.; Stanton, J. F.; McMahon, R. J. *J. Am. Chem. Soc.* **1997**, *119*, 5847.
(29) Clauberg, H.; Minsek, D. W.; Chen, P. *J. Am. Chem. Soc.* **1992**, *114*, 99.
(30) Fahr, A.; Hassanzadeh, P.; Laszlo, B.; Huie, R. E. *Chem. Phys.* **1997**, *215*, 59.
(31) Rabalais, J. W.; McDonald, J. M.; Scherr, V.; McGlynn, S. P. *Chem. Rev.* **1971**, *71*, 73.
(32) Jackson, W. M.; Anex, D. S.; Continetti, R. E.; Balko, B. A.; Lee, Y. T. *J. Chem. Phys.* **1991**, *95*, 7327.
(33) Sun, W.; Yokoyama, K.; Robinson, J. C.; Suits, A. G.; Neumark, D. M. *J. Chem. Phys.* **1999**, *110*, 4363.
(34) Song, X.; Bao, Y.; Urdahl, R. S.; Gosine, J. N.; Jackson, W. M. *Chem. Phys. Lett.* **1994**, *217*, 216.
(35) Jackson, W. M.; Mebel, A. M.; Lin, S. H.; Lee, Y. T. *J. Phys. Chem. A* **1997**, *101*, 6638.
(36) Mebel, A. M.; Jackson, W. M.; Chang, A. H. H.; Lin, S. H. *J. Am. Chem. Soc.* **1998**, *120*, 5751.
(37) Ni, C.-K.; Huang, J.-D.; Chen, Y.-T.; Kung, A. H.; Jackson, W. M. *J. Chem. Phys.* **1999**, *110*, 3320.
(38) Wiley, W. C.; McClaren, I. H. *Rev. Sci. Instrum.* **1955**, *26*, 1150.
(39) Pearse, R. W. B.; Gaydon, A. G. *The Identification of Molecular Spectra*; Chapman and Hall: London, 1976.
(40) Huber, K. P.; Herzberg, G. *Molecular Spectra and Molecular Structure IV. Constants of Diatomic Molecules*; Van Nostrand Reinhold: New York, 1979.
(41) Bashkin, S.; Stoner, J. D., Jr. *Atomic Energy Levels and Grotrian Diagrams*; North-Holland: Amsterdam, 1975.
(42) Martin, M. *J. Photochem. Photobiol. A* **1992**, *66*, 263.
(43) Spindler, R. J. *J. Quant. Spectrosc. Radiat. Transfer* **1965**, *5*, 165.
(44) Lin, S. H.; Fujimura, Y.; Neusser, H. J.; Schlag, E. W. *Multiphoton Spectroscopy of Molecules*; Academic: Orlando, FL, 1984.
(45) Rohlfing, E. A.; Cox, D. M.; Kaldor, A. *J. Chem. Phys.* **1984**, *81*, 3322.
(46) Ramanathan, R.; Zimmerman, J. A.; Eyler, J. R. *J. Chem. Phys.* **1993**, *98*, 7838.
(47) Lemire, G. W.; Fu, Z.; Hamrick, Y. M.; Taylor, S.; Morse, M. D. *J. Phys. Chem.* **1989**, *93*, 2313.
(48) Yang, Z. Z.; Wang, L. S.; Lee, Y. T.; Shirley, D. A.; Huang, S. Y.; Lester, W. A., Jr. *Chem. Phys. Lett.* **1990**, *171*, 9.
(49) Minsek, D. W.; Chen, P. *J. Phys. Chem.* **1990**, *94*, 8399.
(50) Franklin, J. L.; Mogenis, A. *J. Phys. Chem.* **1967**, *71*, 2820.
(51) Rothberg, L. J.; Gerrity, D. P.; Vaida, V. *J. Chem. Phys.* **1981**, *75*, 4403.
(52) Fahr, A.; Hassanzadeh, P.; Laszlo, B.; Huie, R. E. *Chem. Phys.* **1997**, *215*, 59.
(53) Bokor, J.; Zavelovich, J.; Rhodes, C. K. *J. Chem. Phys.* **1980**, *72*, 965.
(54) Meijer, G.; Wodtke, A. M.; Voges, H.; Schlüter, H.; Andresen, P. *J. Chem. Phys.* **1988**, *89*, 2588.
(55) Hill, W. T., III; Turner, B. P.; Lefebvre-Brion, H.; Yang, S.; Zhu, J. *J. Chem. Phys.* **1990**, *92*, 4272.
(56) Turner, B. P.; Hill, W. T., III; Yang, S.; Zhu, J.; Pinkas, A.; Bao, L. *Rev. Sci. Instrum.* **1990**, *61*, 1182.
(57) Merrow, C. N.; Forch, B. E. *J. Chem. Phys.* **1990**, *93*, 4791.
(58) Forch, B. E.; Merrow, C. N. *J. Chem. Phys.* **1991**, *95*, 3252.